Tetrahedron 65 (2009) 7653–7657

Contents lists available at ScienceDirect

Tetrahedron

journal homepage: www.elsevier.com/locate/tet

Acyl radical addition to pyridine: multiorbital interactions

Ruth I.J. Amos [a], Jason A. Smith [a], Brian F. Yates [a], Carl H. Schiesser [b,c,*]

[a] School of Chemistry, University of Tasmania, Private Bag 75, Hobart, Tasmania, 7001, Australia
[b] School of Chemistry, The University of Melbourne, Victoria 3010, Australia
[c] Bio21 Molecular Science and Biotechnology Institute, The University of Melbourne, Victoria 3010, Australia

ARTICLE INFO

Article history:
Received 19 March 2009
Received in revised form 7 June 2009
Accepted 25 June 2009
Available online 2 July 2009

Keywords:
Acyl radical
Homolytic addition
Dual orbital effect
Pyridine
Pyridinium

ABSTRACT

The addition of the acetyl radical at the various positions in both pyridine and the pyridinium ion has been investigated using DFT calculations. Additions at the 2-, 3- and 4-positions in these systems are associated with simultaneous SOMO→π* and π→SOMO interactions, with the former interaction dominating in the case of pyridine, and that latter in the case of pyridinium. Simultaneous SOMO→π*, LP_N→SOMO and LP_N→$\pi^*_{c=o}$ interactions are predicted for the addition at the nitrogen atom in pyridine. The energy barrier for attack at the nitrogen atom in pyridine is calculated to be 54 kJ mol^{-1} at the BHandHLYP/6-311G(d,p) level of theory, some 6 kJ mol^{-1} lower than for the analogous attack at any other atom in pyridine, or at any position in the pyridinium ion. Multiorbital interactions are responsible this preference, resulting in an unusual motion vector in the transition state for attack at the nitrogen atom in pyridine.

1. Introduction

Isoniazid (**1**), the hydrazide of isonicotinic acid, is an important antibiotic used to combat tuberculosis (TB).[1] Increasingly *Mycobacterium tuberculosis* is becoming resistant to the antibiotics used for its treatment, including **1**. It is therefore important that the mode of action of isoniazid is better understood in order to combat this drug resistance.[1,2]

Isoniazid **1** is a prodrug which is activated to form a reactive intermediate which then adds to the biological cofactor NAD^+ to form the 'true drug' (**2**, Scheme 1).[3] This activation is carried out in the bacterium by the catalase-peroxidase enzyme KatG.[4–9] Electron spin resonance (ESR) studies have suggested that free radicals are the intermediates involved in this process.[6] Recently we reported studies supporting the hypothesis that the reactive intermediate formed is the acyl radical produced by oxidation of **1**.[10] An important step in the chemistry of isoniazid is the addition of this intermediate radical to the pyridinium ion in NAD^+ to form **2** (Scheme 1).

Acyl radicals have traditionally been thought to be nucleophilic in their addition to alkenes.[11] Recent results, however, suggest that acyl radicals can also act as electrophilic radicals depending on the electronic demand of the π-system undergoing addition, as well as deriving assistance during addition chemistry by masquerading as electrophiles.[12] Given the similarities to previous work, we were interested in determining whether or not these interactions are also important in the isoniazid chemistry described above. To that end, we now report our computational results for the addition of acetyl radicals to the pyridinium ion and pyridine.

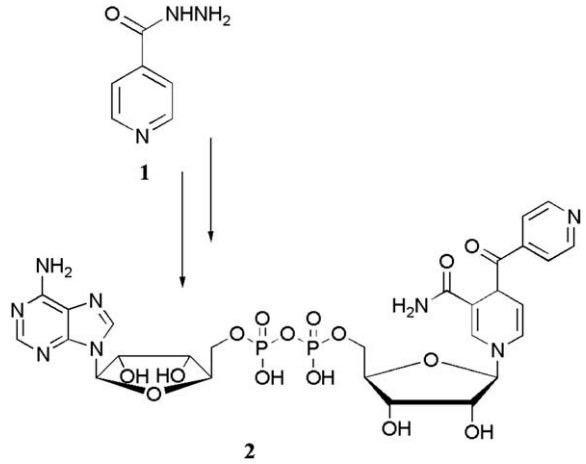

Scheme 1. The addition of isoniazid (**1**) to NAD^+ to form the true drug (**2**).

2. Computational methods

Previous benchmarking studies[12,13] established that BHandHLYP/6-311G(d,p) is a reliable level of theory for the study of the reactions of acyl radicals with π-bonds, so we chose to use this method in this study.

* Corresponding author. Tel.: +613 83442430; fax: +613 93478189.
E-mail address: director@freeradical.org.au (C.H. Schiesser).

0040-4020/$ – see front matter © 2009 Elsevier Ltd. All rights reserved.
doi:10.1016/j.tet.2009.06.102

Geometry optimizations were performed using the Gaussian 03 program[14] at BHandHLYP/6-311G(d,p). An unrestricted method was used for the open-shell systems. Ground and transition state structures were verified using vibrational frequency analysis, also at the BHandHLYP/6-311G(d,p) level of theory. Zero point vibrational energy corrections have been applied to all structures. Natural Bond Orbital (NBO) analyses were carried out using NBO 5.0[15] linked through the Gaussian 03 program.

Optimised geometries and energies for all transition structures as well as an avi of the interesting transition structure vector are available as Supplementary data.

3. Results and discussion

3.1. Reaction of acetyl radical with the pyridinium ion

Structures **3**–**6** are the lowest energy transition structures found at the BHandHLYP/6-311G(d,p) level of theory for the reaction of the acetyl radical at the N1, C2, C3 and C4 positions of the pyridinium ring respectively (Fig. 1). Separations of the reacting units in these transition structures are predicted to be larger for attack on the carbon than on the nitrogen. For example, the attack on C2 (**4**, Fig. 1) is predicted to have a separation of 2.161 Å which is larger than 2.001 Å for the attack at the nitrogen (**3**, Fig. 1). The angles (θ) around the carbonyl bond are predicted to change according to the electron density on the ring. The angle of attack is 109.8° for the nitrogen (**3**, Fig. 1) where electron density is low as compared to 114.0° at C3 (**5**, Fig. 1) where there is the greatest electron density.

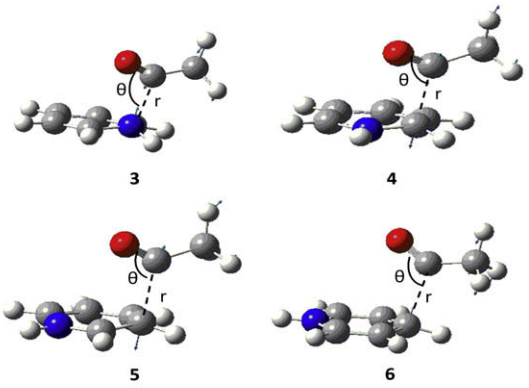

	r	θ
3	2.001Å	109.8°
4	2.161Å	110.3°
5	2.114Å	114.0°
6	2.215Å	112.1°

Figure 1. BHandHLYP/6-311G(d,p) optimized structures of transition states **3**, **4**, **5** and **6** for the homolytic addition of the acetyl radical to the pyridinium ion at the N1, C2, C3 and C4 positions.

Table 1 lists the energy barriers for the forward ($\Delta E_1^{\ddagger}$) and reverse ($\Delta E_2^{\ddagger}$) reactions of addition of the acetyl radical to the pyridinium ion. Examination of this table reveals that the addition of the acetyl radical to pyridinium is thermodynamically unfavourable.

Table 1
Calculated energy barriers for the forward ($\Delta E_1^{\ddagger}$) and reverse ($\Delta E_2^{\ddagger}$) reactions of the acetyl radical with the pyridinium ion

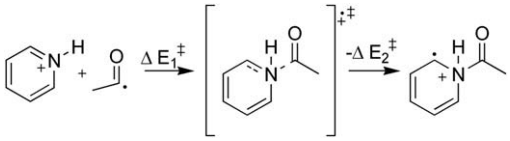

Transition Structure	$\Delta E_1^{\ddagger}$	$\Delta E_1^{\ddagger}$+ZPE	$\Delta E_2^{\ddagger}$	$\Delta E_2^{\ddagger}$+ZPE	ν_i
3	138.1	134.9	8.2	4.9	231*i*
4	72.4	72.2	46.3	41.7	262*i*
5	99.0	97.5	38.6	35.1	355*i*
6	68.9	69.1	19.0	16.6	182*i*

Inspection of the natural bond orbital (NBO) analysis data for the attack of the acetyl radical at the C2 position of the pyridinium ion (**4**) reveals an interaction between the radical (SOMO) and the π* system of the aromatic ring worth 264 kJ mol^{-1} (Table 2, Fig. 2,**a**), evident in the set of α spin orbitals. An interaction worth 171 kJ mol^{-1} between the π system in the aromatic ring and the unoccupied β component of the SOMO of the radical is evident in the β spin set (Table 2, Fig. 2, b). Similar interactions are found at all

Table 2
Energies of interactions between molecular orbitals for attack at the various positions on both the pyridinium ion and pyridine

Attack via transition state	Figure 2a	Figure 2b	Figure 2c
	SOMO–π* kJ mol^{-1}	π–SOMO kJ mol^{-1}	π_{ar}–$\pi^*_{C=O}$ kJ mol^{-1}
3	816	295	59
4	264	171	
5	274	252	
6	534	346	
8	506	600	
9	492	617	
10	294	319	

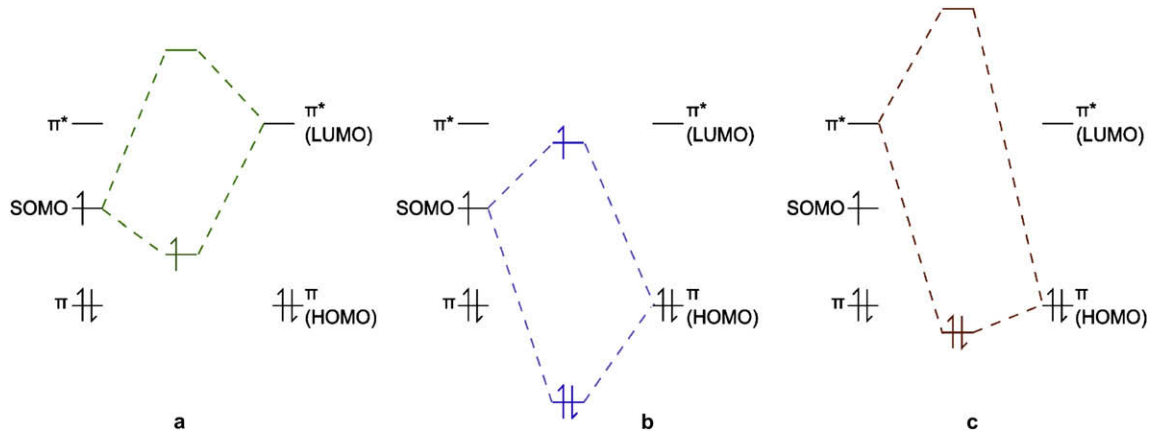

Figure 2. Representative energy diagrams for orbital interactions involved in the homolytic addition of the acetyl radical to the pyridinium ion via transition states **3**, (**a**, **b** and **c**) and **4**, **5** and **6** (**a** and **b** only). The attacks on pyridine via transition states **8**, **9** and **10** are also represented by **a** and **b**.

positions on the pyridinium ring (Table 2, Fig. 2, a and b) indicating that the acetyl radical is more nucleophilic than electrophilic in character when attacking pyridinium. Figure 3 depicts representative transition state orbitals involved during the attack of acetyl radical at the N1 and C2 positions at this level of theory.[16]

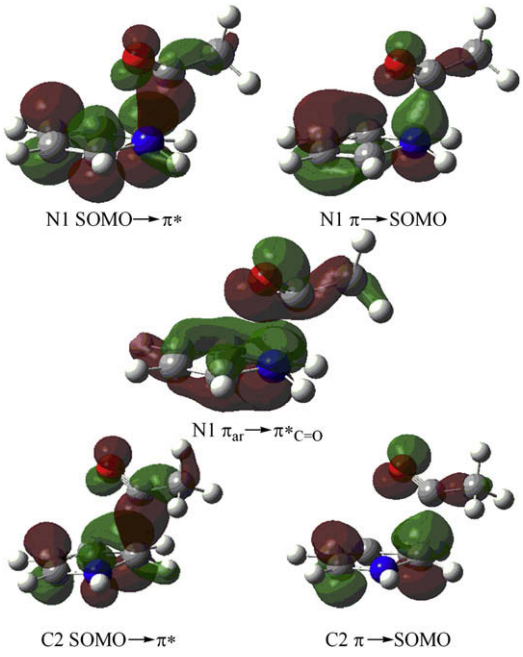

Figure 3. Key BHandHLYP/6-311G(d,p) generated molecular orbitals involved in the homolytic addition of acetyl radical to the N1 and C2 positions of the pyridinium ion.[16]

When the acetyl radical is attacking at the nitrogen of the pyridinium ion (**3**, Fig. 1) there is a slightly more complex interaction pattern found in the NBO analysis. The SOMO→π* interaction in the set of α spin orbitals is worth 816 kJ mol^{-1} (Table 2, Fig. 2**a**) and is the most significant interaction indicating again the nucleophilic nature of the radical in this circumstance. The π→SOMO interaction is evident in both the α (109 kJ mol-1) and β (187 kJ mol^{-1}) spin sets (Table 2, Fig. 2,**b**) and a further small π$_{aromatic}$→π*C=O interaction worth 42 kJ mol^{-1} (α) and 17 kJ mol^{-1} (β) is also present (Table 2, Fig. 2,**c**).

3.2. Reaction of acetyl radical with pyridine

Structures **7**, **8**, **9** and **10** (Fig. 4) are the lowest energy transition structures found for the reaction of the acetyl radical at the N1, C2, C3 and C4 positions on the pyridine ring respectively. Once again the separation of the reactants in the transition state is shorter for attack on the nitrogen (1.817 Å for **7** vs 2.087 Å for attack at the C2 position, **8**) and in this case the angle of attack is quite different (109.4° for **7** vs 119.6° for **8**). The angles of attack for the carbons follow the electron density of pyridine with the largest angle on the C2 and smallest on the C3 position.

Table 3 lists the energy barriers for the forward and reverse reactions for addition of the acetyl radical to pyridine. Inspection of these data reveals that the forward reaction for addition of the radical to the nitrogen in pyridine ($\Delta E_1^{\ddagger}$, **7**) is 5.5 kJ mol^{-1} more favourable than addition at any other part of the ring in that it has a calculated energy barrier of 53.5 kJ mol^{-1} compared to 59.0 kJ mol^{-1} for the nearest neighbour. The calculated energy barriers for the reverse reactions are similar to the forward barriers and it is only the addition to the nitrogen on the pyridine that there is a significant preference for the forward reaction ($\Delta E_2^{\ddagger}$ **7**=132.5 kJ mol^{-1}).[17]

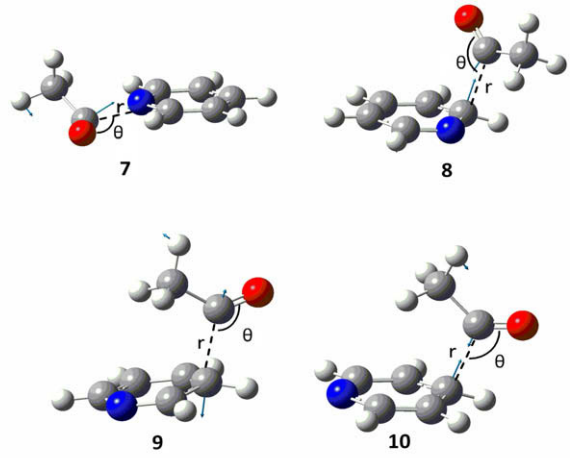

	r	θ
7	1.817Å	109.4°
8	2.087Å	119.6°
9	2.093Å	115.9°
10	2.087Å	116.0°

Figure 4. BHandHLYP/6-311G(d,p) optimized structures of transition states **7**, **8**, **9** and **10** for the homolytic addition of the acetyl radical to pyridine at the N1, C2, C3 and C4 positions respectively.

Table 3
Calculated energy barriers for the forward ($\Delta E_1^{\ddagger}$) and reverse ($\Delta E_2^{\ddagger}$) reactions of the acetyl radical with pyridine

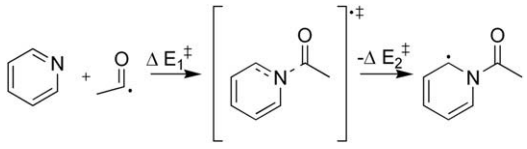

Transition Structure	$\Delta E_1^{\ddagger}$	$\Delta E_1^{\ddagger}$+ZPE	$\Delta E_2^{\ddagger}$	$\Delta E_2^{\ddagger}$+ZPE	ν_i
7	50.5	53.5	137.7	132.5	494*i*
8	64.4	63.0	73.2	68.6	479*i*
9	65.0	64.5	69.3	64.9	514*i*
10	58.5	59.0	61.6	57.4	461*i*

Insight into the attack trajectory of the acetyl radical is found by investigating the transition state vector; this information is included as motion arrows in Figure 4. Whilst the vectors for the transition structures associated with addition at the C2, C3 and C4 are as expected for homolytic addition to a π-system (Figs. 4 and 5), the vector for transition structure **7** is unusual in that it shows movement that corresponds to a rocking motion when visualized using a program such as GaussView. This signifies a more complex set of orbital interactions (Figs. 4 and 5) and is similar to motion vectors associated with attack of the acetyl radical and the oxyacyl radical at the nitrogen end of imines.[12,18]

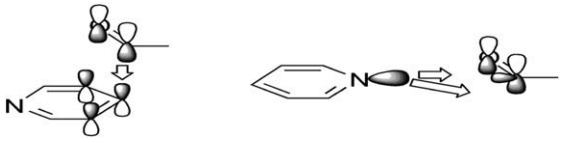

Figure 5. Alignment of orbitals for addition to pyridine.

The NBO data for attack of the acetyl radical at the C2 (**8**), C3 (**9**) and C4 (**10**) positions of pyridine reveals that the radical is now electrophilic in character. The C2 attack (**8**) gives a SOMO→π*

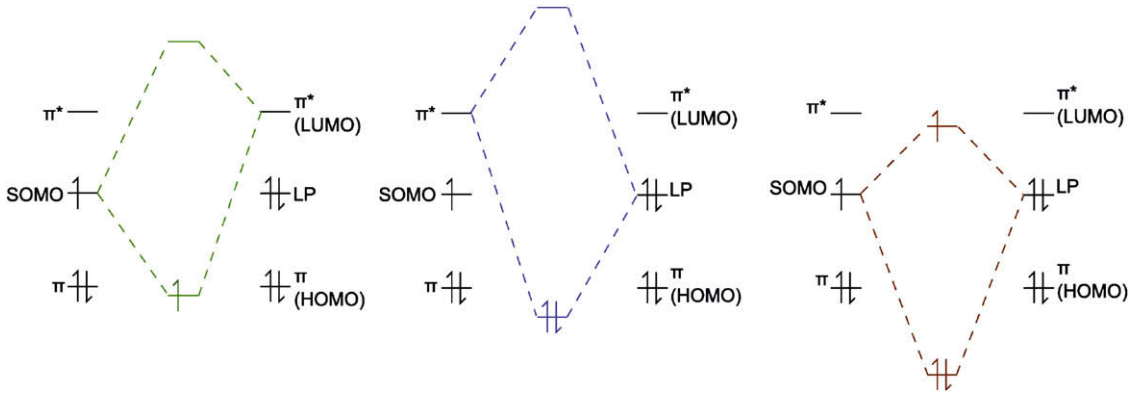

Figure 6. Representation of the orbital interactions between the acetyl radical and pyridine at the nitrogen.

interaction worth 121 kJ mol^{-1} in the set of α spin orbitals, while the β spin set furnishes a π→SOMO interaction worth 143 kJ mol^{-1}. Attack on the C3 (**9**) and C4 (**10**) positions show a similar effect (Fig. 2, Table 2).

The NBO data for the attack on the nitrogen of the pyridine ring (**7**) also shows the electrophilic character of this radical, and in addition indicates a reason for the rocking motion found in the transition state. In this case the lone pair of the nitrogen is involved in the bonding rather than the π system of the aromatic ring (Fig. 6). The LP→SOMO interactions are worth 377 kJ mol^{-1} (β spin set) and LP→LUMO interactions are 205 kJ mol^{-1} (α spin set) and 71 kJ mol^{-1} (β spin set), while the SOMO→π* interaction is only worth 75 kJ mol^{-1} (Fig. 6). It is the combination of interactions that maximizes the energy gain from orbital interactions and is responsible for the rocking motion as described in Figures 4 and 5. Figure 7 also depicts the orbitals involved in these transition states for the attacks on pyridine.[16]

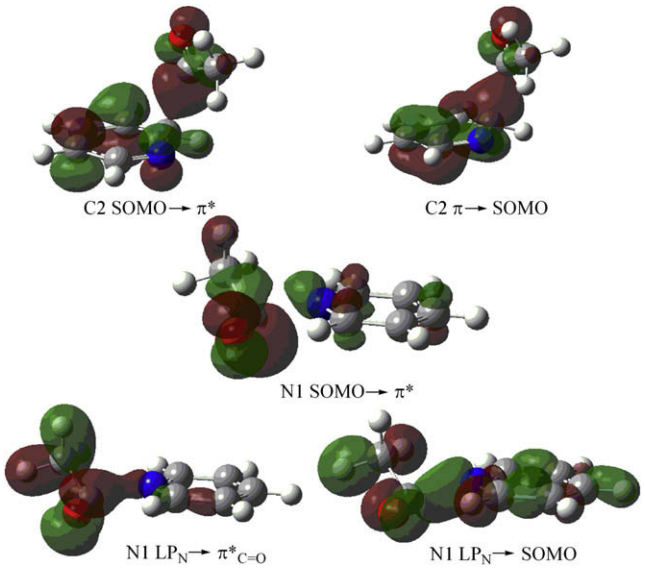

Figure 7. Key BHandHLYP/6-311G(d,p) generated molecular orbitals involved in the homolytic addition of acetyl radical to the N1 and C2 positions of pyridine.[16]

3.3. NAD$^+$ model

The calculated barriers for the addition of the acetyl radical to pyridinium suggest that this reaction is endothermic. In order to model the formation of **2** more closely, we chose to examine the addition of the acetyl radical to the 2-carbamidopyridinium ion (**11**). This model (Scheme 2) was chosen as it more closely

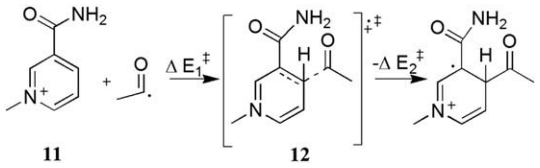

Scheme 2. The model for addition to NAD$^+$.

resembles the pyridinium ring in NAD+. These calculations reveal that this chemistry is predicted to be exothermic by 27.0 kJ mol^{-1} compared to the parent reaction which is caluclated to be endothermic by 52.3 kJ mol^{-1}. In addition, the energy barrier ($\Delta E_1^{\ddagger}$) is reduced to 21.4 kJ mol^{-1} for the reaction involving **11** (from 69.1 kJ mol^{-1} for the parent). It is clear that the increased electron withdrawing ability afforded by the amide group on the pyridinium ring is necessary for homolytic addition to occur readily. This observation is in agreement with the observation that the acetyl radical behaves in a nucleophilic manner with pyridinium ions (see above). It is also consistent with the data of Minisci and co-workers who report that the addition of one acyl radical to a pyridinium ring strongly activates the ring to further substitution.[19]

4. Conclusions

In agreement with earlier calculations, the acetyl radical is calculated to be ambiphilic in nature, reacting as a nucleophilic radical with pyridinium ions, and as an electrophilic radical with pyridine. Interestingly, attack at the nitrogen atom in pyridine involves multiorbital interactions that are responsible for the unusual motion vectors associated with the transition state for this reaction. Incorporation of an electron-withdrawing amide functionality on the pyridinium ring accelerates these reactions and is likely to be responsible for the chemistry observed for NAD$^+$.

Acknowledgements

Support of the Australian Research Council through the Centres of Excellence Program is gratefully acknowledged. RIJA thanks the University of Tasmania and the Australian Government for an APA. We thank TPAC for computer time.

Supplementary data

The following are available as Supplementary data. Optimised geometries (Gaussian archive entries) of structures **3**–**10** and **12**. Gaussview generated animation of the transition state vector in **7** as an Audio Video Interleave (AVI) file. Supplementary data associated with this article can be found in the online version, at doi:10.1016/j.tet.2009.06.102.

References and notes

1. Rouhi, A. M. *Chem. Eng. News* **1999**, *77*, 52–69.
2. Bloom, B. R.; Murray, C. J. *Science* **1992**, *257*, 1055–1064.
3. Rozwarski, D. A.; Grant, G. A.; Barton, D. H. R.; Jacobs, W. R., Jr.; Sacchettini, J. C. *Science* **1998**, *279*, 98–102.
4. Lukat-Rodgers, G. S.; Wengenack, N. L.; Rusnak, F.; Rodgers, K. R. *Biochemistry* **2001**, *40*, 7149–7157.
5. Wengenack, N.; Hoard, H. M.; Rusnak, F. *J. Am. Chem. Soc.* **1999**, *121*, 9748–9749.
6. Wengenack, N.; Rusnak, F. *Biochemistry* **2001**, *40*, 8990–8996.
7. Saint-Joanis, B.; Souchon, H.; Wilming, M.; Johnsson, K.; Alzari, P. M.; Cole, S. T. *Biochem. J.* **1999**, *338*, 753–760.
8. Ghiladi, R. A.; Medzihradszky, K. F.; Rusnak, F. M.; Ortiz de Montellano, P. R. *J. Am. Chem. Soc.* **2005**, *127*, 13428–13442.
9. Zhao, X.; Yu, H.; Yu, S.; Wang, F.; Sacchettini, J. C.; Magliozzo, R. S. *Biochemistry* **2006**, *45*, 4131–4140.
10. Amos, R. I. J.; Gourlay, B. S.; Schiesser, C. H.; Smith, J. A.; Yates, B. F. *Chem. Commun.* **2008**, 1695–1697.
11. Chatgilialoglu, C.; Crich, D.; Komatsu, M.; Ryu, I. *Chem. Rev.* **1999**, *99*, 1991–2069.
12. Kyne, S. H.; Schiesser, C. H.; Matsubara, H. *J. Org. Chem.* **2008**, *73*, 427–434.
13. Schiesser, C. H.; Matsubara, H.; Ritsner, I.; Wille, U. *Chem. Commun.* **2006**, 1067–1069.
14. Frisch, M. J.; Trucks, G. W.; Schlegel, H. B.; Scuseria, G. E.; Robb, M. A.; Cheeseman, J. R.; Montgomery, J. A., Jr.; Vreven, T.; Kudin, K. N.; Burant, J. C.; Millam, J. M.; Iyengar, S. S.; Tomasi, J.; Barone, V.; Mennucci, B.; Cossi, M.; Scalmani, G.; Rega, N.; Petersson, G. A.; Nakatsuji, H.; Hada, M.; Ehara, M.; Toyota, K.; Fukuda, R.; Hasegawa, J.; Ishida, M.; Nakajima, T.; Honda, Y.; Kitao, O.; Nakai, H.; Klene, M.; Li, X.; Knox, J. E.; Hratchian, H. P.; Cross, J. B.; Bakken, V.; Adamo, C.; Jaramillo, J.; Gomperts, R.; Stratmann, R. E.; Yazyev, O.; Austin, A. J.; Cammi, R.; Pomelli, C.; Ochterski, J. W.; Ayala, P. Y.; Morokuma, K.; Voth, G. A.; Salvador, P.; Dannenberg, J. J.; Zakrzewski, V. G.; Dapprich, S.; Daniels, A. D.; Strain, M. C.; Farkas, O.; Malick, D. K.; Rabuck, A. D.; Raghavachari, K.; Foresman, J. B.; Ortiz, J. V.; Cui, Q.; Baboul, A. G.; Clifford, S.; Cioslowski, J.; Stefanov, B. B.; Liu, G.; Liashenko, A.; Piskorz, P.; Komaromi, I.; Martin, R. L.; Fox, D. J.; Keith, T.; Al-Laham, M. A.; Peng, C. Y.; Nanayakkara, A.; Challacombe, M.; Gill, P. M. W.; Johnson, B.; Chen, W.; Wong, M. W.; Gonzalez, C.; Pople, J. *A Gaussian 03, Revision D.01*; Gaussian: Wallingford, CT, 2004.
15. Glendening, E. D.; Badenhoop, J. K.; Reed, A. E.; Carpenter, J. E.; Bohmann, J. A.; Morales, C. M.; Weinhold, F. *NBO5.0*; Theoretical Chemistry Institute: University of Wisconsin: Madison, WI, 2001.
16. The BHandHLYP/6-311G(d,p) generated molecular orbitals for the C2 position are representative of the key orbitals generated for the C3 and C4 positions.
17. These results are consistent with our experimental results in that the formation of acyl radicals from the oxidation of hydrazides by a manganese catalyst in pyridine gave no acylated pyridine products. (See ref. 10 for details).
18. Kyne, S. H.; Schiesser, C. H.; Matsubara, H. *Org. Biomol. Chem.* **2007**, *5*, 3938–3943.
19. Fontana, F.; Minisci, F.; Nogueira Barbosa, M. C.; Vismara, E. *J. Org. Chem.* **1991**, *56*, 2866–2869.